Fabrication of highly spin-polarized $Co_2FeAl_{0.5}Si_{0.5}$ thin-films

M. Vahidi, J. A. Gifford, S. K. Zhang, S. Krishnamurthy, Z. G. Yu, L. Yu, M. Huang, C. Youngbull, T. Y. Chen, and N. Newman'

Articles you may be interested in

Preparation and characterization of highly $L2_1$-ordered full-Heusler alloy $Co_2FeAl_{0.5}Si_{0.5}$ thin films for spintronics device applications
Applied Physics Letters **92**, 221912 (2008); 10.1063/1.2940595

Tunnel magnetoresistance for junctions with epitaxial full-Heusler $Co_2FeAl_{0.5}Si_{0.5}$ electrodes with $B2$ and $L2_1$ structures
Applied Physics Letters **89**, 112514 (2006); 10.1063/1.2354026

Perspective: n-type oxide thermoelectrics via visual search strategies
APL Materials **4**, 053201 (2016); 10.1063/1.4941711

Perspectives for spintronics in 2D materials
APL Materials **4**, 032401 (2016); 10.1063/1.4941712

Isotropic, high coercive field in melt-spun tetragonal Heusler Mn_3Ge
APL Materials **4**, 086113 (2016); 10.1063/1.4961660

Large tunnel magnetoresistance in $Co_2FeAl_{0.5}Si_{0.5} / MgO / Co_2FeAl_{0.5}Si_{0.5}$ magnetic tunnel junctions prepared on thermally oxidized Si substrates with MgO buffer
Applied Physics Letters **93**, 182504 (2008); 10.1063/1.3020300

Fabrication of highly spin-polarized $Co_2FeAl_{0.5}Si_{0.5}$ thin-films

M. Vahidi,[1] J. A. Gifford,[2] S. K. Zhang,[1] S. Krishnamurthy,[3] Z. G. Yu,[3] L. Yu,[1] M. Huang,[1] C. Youngbull,[4] T. Y. Chen,[2] and N. Newman[1,a]

[1]*School of Materials, Arizona State University, Tempe, Arizona 85287-8706, USA*
[2]*Department of Physics, Arizona State University, Tempe, Arizona 85287, USA*
[3]*SRI International, 301-64, Menlo Park, California 94025, USA*
[4]*The Biodesign Institute, Arizona State University, Tempe, Arizona 85287, USA*

Ferromagnetic Heusler $Co_2FeAl_{0.5}Si_{0.5}$ epitaxial thin-films have been fabricated in the $L2_1$ structure with saturation magnetizations over 1200 emu/cm^3. Andreev reflection measurements show that the spin polarization is as high as 80% in samples sputtered on unheated MgO (100) substrates and annealed at high temperatures. However, the spin polarization is considerably smaller in samples deposited on heated substrates. © *2014 Author(s). All article content, except where otherwise noted, is licensed under a Creative Commons Attribution 3.0 Unported License.* [http://dx.doi.org/10.1063/1.4869798]

The performance of spintronic devices depends on generating highly spin-polarized carrier populations.[1–3] In theory, perfectly spin-aligned carrier populations can be injected from half metals (HF)[4,5] since they have an electronic structure with one spin band at the Fermi level. However, the injection efficiency from most HFs measured to date is far below 100% and is strongly temperature dependent.[6] This presumably arises from the presence of spin-wave excitations and energy band(s) with opposing spin near the Fermi level.[6]

Co-based full-Heusler alloys [7–10] have been proposed for use as electrodes to improve spintronic device performance, although these alloys' spin polarization are typically observed to be below 75% by direct measurements.[11–13] Recently, very large giant magnetoresistance (GMR) values have been inferred from measurements on epitaxial CPP (current perpendicular to film plane)[14,15] and TMR[6,16] structures fabricated with $Co_2FeAl_{0.5}Si_{0.5}$ (CFAS) electrodes. Of particular interest is the large CPP GMR measured in devices with resistances smaller than that found in MgO-based MTJs. This finding may have important implications for hard-drive read-head applications.

The half metallicity of CFAS has been indirectly verified using crystalline MTJs[6,16] and the spin polarization is deduced to be over 90%. This, however, does not prove that the electrodes are highly spin polarized since spin-filtering during transport can occur from the coherent tunneling and interface scattering processes.[17] This effect is well documented in MRAM devices using Fe electrodes and MgO tunnel barriers where the current is almost 100% spin polarized,[18] eventhough Fe is known to have a spin polarization of ∼50% at the Fermi level.[19] Thus, a direct measurement of the intrinsic spin polarization of the CFAS is imperative both to understand the origin of the large CFAS-based GMR and TMR and to improve the performance of CFAS-based spintronic devices.

In this Letter, we report the results of our systematic study to understand the effect of the growth method and thermal processing on the spin polarization in CFAS. We directly measure the spin polarization using Andreev reflection (AR) spectroscopy in point–contact and vertical tunnel junction configurations. We show that the extent of polarization of the injected charge carriers depends strongly on the growth method used and the thermal processing conditions. We observe a spin polarization value as high as 80% in samples sputtered on unheated MgO (100) substrates and

---

[a]Author to whom correspondence should be addressed. Electronic mail: Nathan.Newman@asu.edu

in situ annealed at high temperatures. These results are expected to be useful for the development of spintronic devices with improved performance.

CFAS films were synthesized using magnetron sputtering on MgO (100) substrates in a cryo-pumped ultra-high vacuum (UHV) chamber with an unbaked base pressure of 2×10^{-8} Torr. For comparison, a few films were grown using pulsed laser deposition in a similarly equipped system. Stoichiometric $Co_2FeAl_{0.5}Si_{0.5}$ polycrystalline targets were used for both growth methods. Sputtered films were grown in 5 mTorr Argon gas at a plasma power of 100 W, while pulsed laser deposition films were grown in 5 mTorr Ar with a frequency of 10 Hz and 450 mJ/pulse excimer laser power. Rutherford backscattered spectroscopy (RBS) measurements and analysis were used to infer the composition and thickness of the thin-films. High-resolution x-ray diffraction (PANalytical X'Pert PRO) was used for structural characterization. The magnetic properties of the films were characterized using a vibrating sample magnetometer (VSM) from 4–1000 K (Quantum Design, Model PPMS with oven option). An atomic force microscope (Veeco, Dimension 300) was used to measure the surface quality and roughness of the thin-films.

We undertook two growth processes—1-step and 2-step processes—to compare and optimize the structural and magnetic properties of the CFAS thin-films. CFAS was deposited at an elevated growth temperature (T_g) in the 1-step process, whereas it was deposited at room temperature (RT) and then *in situ* annealed at higher temperature (T_a) in the 2-step process.

Spin polarization values (*P*) of the CFAS films were measured by point contact Andreev reflection (PCAR) operated at 4.2 K using superconducting Pb tips. Vertical Pb superconductor/insulating barrier/CFAS thin-film trilayer junctions were also fabricated and characterized. To form the device, two types of tunnel barrier layers were prepared on 50 nm thick CFAS layers: (a) a CFAS native oxide produced by air-exposure, and (b) an AlO_x layer produced by oxidizing a $\sim$4 nm Al layer deposited *in situ* on an ion-milled CFAS surface.[20] Then a 1 mm wide barrier/CFAS strip was patterned using photolithography and reactive Ar ion etching (RIE). A Ge layer was then deposited at RT over the entire substrate, except on top of the barrier/CFAS strip, to act as a low temperature insulator to prevent shorting between electrodes. Finally, the 200 nm thick Pb layer was deposited using thermal evaporation through a shadow mask. The electrical characteristics of the device were measured using a 4-point measurement with a dipping probe in a liquid He Dewar.

RBS results showed that the CFAS thin-films are stoichiometric and have a thickness of $\sim$50 nm. Figure 1 shows the effect of annealing and growth temperature on the magnetic moment (μ_B), magnetization (M_s), coercive field (H_c), and resistivity (ρ) of sputtered thin-films synthesized in 1-step and 2-step processes. The saturation magnetization is found, in general, to increase with both annealing (2-step) and growth temperaure (1-step), as shown in Fig. 1(a). The saturation magnetization of >1200 emu/cm^3 was achieved with both 1-step and 2-step processes. This corresponds to a moment of $\sim$6 μ_B for both growth methods when $T_g = T_a = 600\,^\circ$C. According to the Slater-Pauling rule, the CFAS moment is expected to be 5.5 μ_B, although a value of 6 μ_B is expected for nonstoichiometric and structually disordered CFAS material.[21] The coercivity of the samples slightly decreases with increasing T_g or T_a, then increases for T_a and T_g greater than 350 $^\circ$C, as shown in Fig. 1(b). The coercivity was found to be considerably larger for the CFAS films prepared by the 1-step procedure compared to the 2-step procedure when processing temperatures above 350 $^\circ$C were used. The resistivity of the CFAS samples at RT is shown in Fig. 1(c) and it decreases with increasing T_a or T_g due to the formation of enhanced degrees of crystallinity. The magnetization was measured from 4 to 1000 K on a CFAS thin-film prepared using the 2-step process with an annealing temperature of 600 $^\circ$C [Fig. 1(d)]. We fit our data to the empirical equation, $M_s/M_{s0} = (1-(T/T_C)^\alpha)^\beta$, where M_{s0} is the zero-temperature magnetization, T_C is the Curie temperature, and α and β are fitting parameters. As shown in Fig. 1(d), the least squares fit to the data gives a Curie temperature of $\sim$1150 $\pm$ 50 K, with the best fit to the experimental data for α and β of 1.5 and 0.45, respectively. The Curie temperatures for similar Co based Heusler alloys, Co_2MnSi[9] and Co_2FeSi,[10] are 985 and 1100 K, respectively. The magnetic properties of these samples grown by both methods are comparable to the best results reported by Wang *et al.*[16,22] for CFAS films grown on MgO substrates and SiO_x/Si substrates with a 20 nm MgO buffer layer (which ranges from 900 emu/cc to 1160 emu/cc) for samples grown at RT without any post annealing and with 680 $^\circ$C post annealing process, respectively.[16]
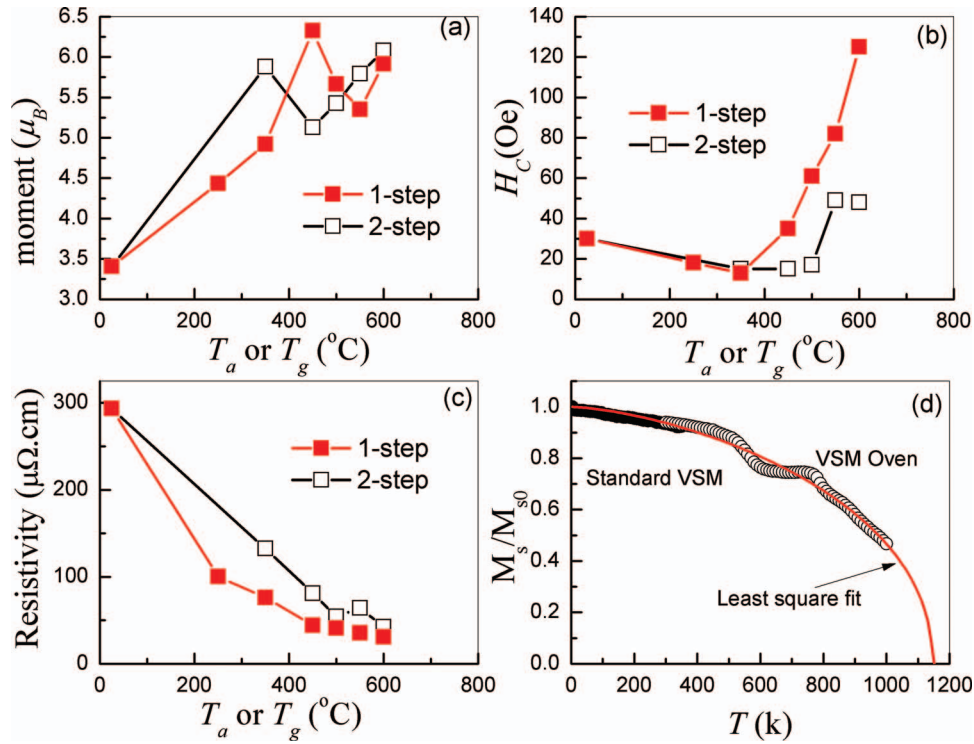
FIG. 1. Magnetic properties and spin polarization of CFAS samples. (a) Magnetic moment, (b) coercivity, and (c) resistivity of films deposited by sputtering as a function of growth and annealing temperatures. (d) Magnetization as a function of temperature for film deposited at RT and annealed at 600 °C.

As illustrated in Fig. 1(c), the room-temperature resistivity for most of the samples is below 100 $\mu\Omega$ cm. We also observed that the resistivity of samples at 4.2 K remains very near that value, with less than a 10% change, which indicates a mean free path of a few nm, as inferred from the Drude model. For each sample, we measured over 10 spectra with contact resistances ranging between 80 Ω and 300 Ω. This corresponds to a contact size of a few nm using the Wexler[23] formula. These values suggest that transport at the contact is close to the ballistic regime.

Since the moment of samples grown by both the 1-step and 2-step methods both attain a value of ~6 μ_B, one anticipates they will have similar levels of polarization. The measured AR spectra on representative films are shown in Fig. 2. We analyze the AR spectra using both the modified Blonder-Tinkham-Klapwijk (BTK) [24–27] and the more recent Chen-Tesaonv and Chien (CTC) models.[28] Representative data (open circles), along with the best fit to the CTC model (red solid line) and the best fit to the modified BTK model (blue solid line), are shown in Fig. 2. Since both fits are near identical, the red and the blue curves are indistinguishable to each other and the obtained P values (as listed inside each figure with the designated color) are very similar. The Z factor represents the interfacial scattering [23–27] in both models and r_E corresponds to the additional resistance that occurs when small point contacts are used on high resistivity samples.[26] For the sample grown at 600 °C, the normalized conductance (dI/dV) is ~1.0 at zero bias [Figs. 2(a) and 2(b)]. For the samples annealed at 600 °C, the normalized conductance is below 0.7 at zero bias [Figs. 2(c) and 2(b)]. This indicates a much higher polarization value for samples annealed at 600 °C. The best fits to both models show that the P value of the 2-step sample is about 0.74, while it is below 0.5 for the sample grown by the 1-step process. One also notes that the conductance shoulders, often referred to as Andreev peaks, occur at ~5 mV—a value much larger than the 1.3 meV superconducting gap of the Pb tip at 4.2 K. This is due to the additional contact resistance (r_E) inherent to high resistance films, which has been incorporated in our analysis for both models.
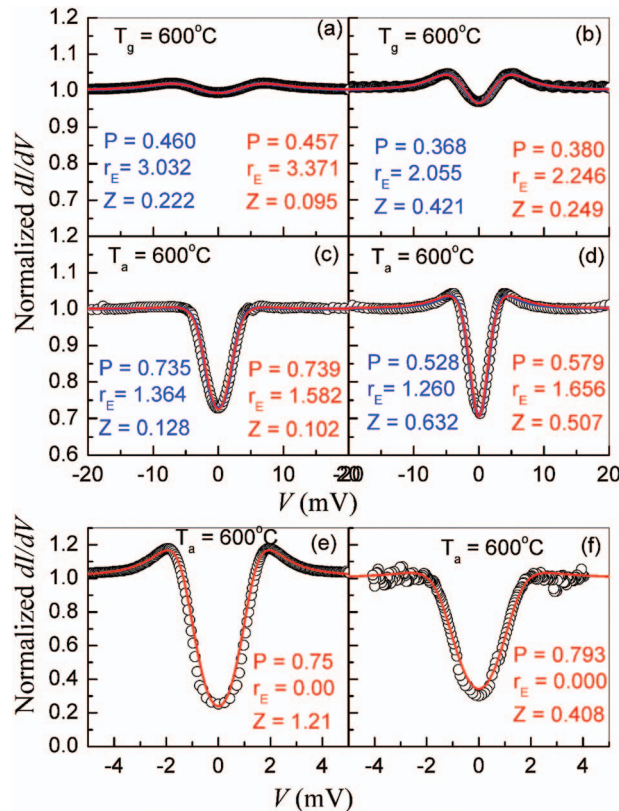
FIG. 2. Representative point contact Andreev reflection spectra of sputtered CFAS samples with different interfacial scattering factors: (a) and (b) sample grown at 600 °C, (c) and (d) sample grown at RT with 600 °C post annealing, (e) and (f) vertical junctions of Pb/Al$_2$O$_3$/CFAS and Pb/native CFAS oxide/CFAS, respectively, with 600 °C post annealed CFAS layer.

Since point-contact AR spectra indicate that samples annealed at 600 °C exhibit the highest polarization value, we fabricated 1×1 mm^2 Pb/insulator (CFAS native oxide or Al$_2$O$_3$)/CFAS trilayer thin-film junctions. The AR spectra of these two junctions are shown in Figs. 2(e) and 2(f). As illustrated in Fig. 2(f), the junction with the native CFAS oxide layer shows no shoulders at the peak, indicative of a smaller barrier at the interface. This can be compared to the Al$_2$O$_3$ oxide layer junction measurements, Fig. 2(e), that show characteristics very close to the tunneling regime. Furthermore, the conductance of both junctions are about 0.3 at zero bias, indicating a high polarization value. Both methods of analysis find that the spin polarization of these junctions is very close to 80%.

The dependence of the P values as a function of the interfacial scattering Z factor for representative samples are shown in Fig. 3. For all the samples, the P values decrease with increasing Z factor due to spin flip scattering at the interface, although there are important differences in the trends. For example, the P value of the sample grown at RT decreases rapidly from 0.47 at Z = 0 to zero at Z ≈ 0.3, Fig. 3(a). In contrast, the P value of the sample annealed at 600 °C (Fig. 3(d)) is higher and is reduced by only a small amount over the same Z range. We also notice that the P values obtained for the trilayer junctions are higher, as shown by the solid squares in Fig. 3(e), and are virtually independent of the Z factor. This can be attributed to higher quality junction interfaces. From the P vs Z curves, one notes that the polarization decreases more rapidly with Z for samples with smaller P values, presumably from stronger spin flip scattering.

By extrapolating to Z = 0 using a polynomial fit (dashed curve), we have obtained the intrinsic P value of each sample. Values for $P(Z = 0)$ are presented in Fig. 3(f). The highest $P(Z = 0)$ is about 80% for the sample annealed at 600 °C. The red solid circle denote the the samples grown with a 2-step pulsed laser deposition (PLD) process that used 550 °C and 780 °C *in situ* anneals. The
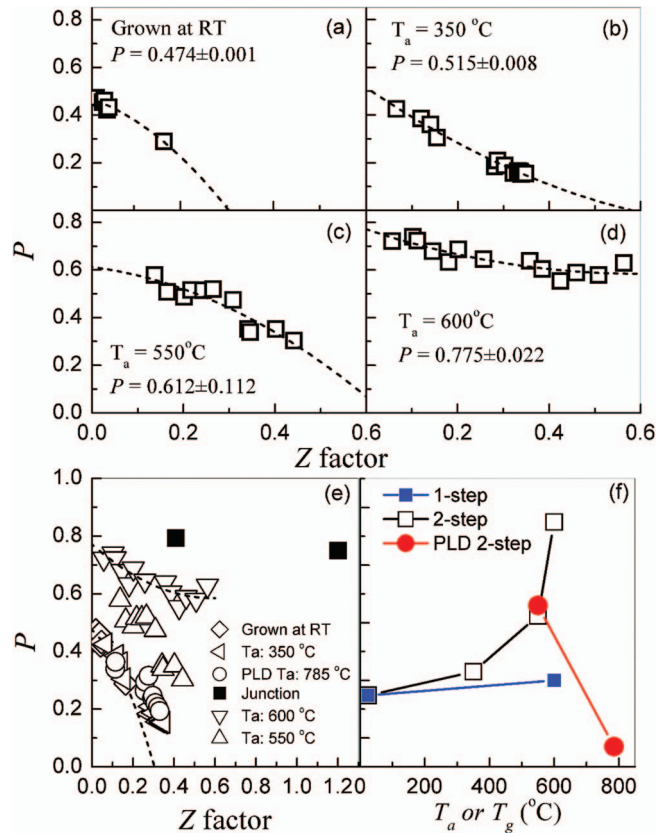
FIG. 3. Representative curves of spin polarization of the sputtered CFAS samples as a function of the interfacial scattering factor Z for (a) sample grown at RT, (b) sample with 350 °C post annealing, (c) sample with 550 annealing, (d) sample with 600 °C annealing, and (e) for all the samples including sample grown by pulsed laser deposition and post annealed at 785 °C. The dashed curves are polynomial fitting. (f) Intrinsic spin polarization $P(Z = 0)$ of samples fabricated by 1-step sputtering, 2-step sputtering and 2-step pulsed laser deposition.

$P(Z = 0)$ value for the sample fabricated with the 2-step sputtering process ($T_a = 550$ °C) is very similar to that grown by PLD, indicating that $P(Z = 0)$ values do not appear to strongly depend on the growth method. However, the $P(Z = 0)$ of the samples grown with the 1-step sputtering process (solid blue square) is much lower. $P(Z = 0)$ is equal to ∼50% for the sputtered sample grown at 600 °C.

We have characterized the films uisng x-ray diffraction (XRD), as shown in Fig. 4. The XRD results indicate that the films grown with the 1-step process are epitaxial when T_g is larger than 250 °C, Fig. 4(a). The intensity of the (002) and (004) CFAS peaks is enhanced with increasing growth temperature, indicating that crystal quality improves under these conditions. XRD Φ scans of the off-axis Bragg peaks have been used to identify the presence of L2$_1$ ordered structure.[16,29] Φ scans of the off-axis CFAS (111) peak on our samples [Fig. 4(a) inset] showed fourfold symmetry in the diffraction patterns. This is direct evidence that films grown at T_g over 350 °C have the L2$_1$ CFAS structure. We conclude that the films are epitaxial with the CFAS L2$_1$ structure and the L2$_1$ ordering improves with increasing growth temperature. It is interesting that these samples show poor spin polarization of ∼50%. A P value of 50% is similar to that measured by ARS on bulk CFAS samples.[21]

We did not detect the presence of epitaxy in the coupled θ-2θ XRD data of films with high P values grown with the 2-step process [Fig. 3(f)]. However, by using XRD grazing angle measurements, we could detect evidence of the polycrystalline CFAS structure with broad XRD Bragg diffraction peaks for film without post annealing [0.7° full width at half maximums (FWHMs) of (220) peak]. The quality of films, as inferred from the intensity and the width of the XRD peaks, was
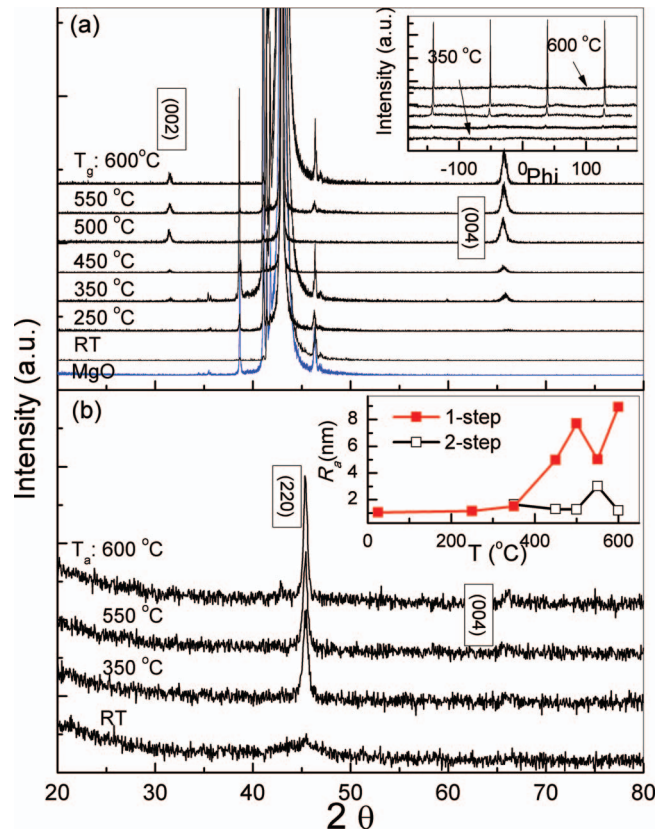
FIG. 4. (a) X-ray θ–2θ diffraction of the CFAS samples fabricated by 1-step method. The inset illustrates the Φ-scans of the off axis (111) peak. (b) XRD grazing angle of the CFAS samples made using the 2-step method. The inset summarizes the roughness of the CFAS samples, as inferred from atomic force microscopy measurements.

found to improve with increasing annealing temperature. The (220) Bragg diffraction peak of the film annealed at 600 °C had a FWHM of 0.46°. Wang *et al.* reported a high spin polarization value of 71% for TMR structure with polycrystalline CFAS electrodes.[16] This value is very similar to the value observed (70%) for CFAS electrodes with B2 ordering structure.[29] In addition, Tezuka *et al.*[29] reported that CFAS MTJs with the highly ordered structure ($L2_1$) have much lower spin polarization than devices containing electrodes with the less ordered structure (B2). The authors attribute the difference in the polarization results to the higher roughness in the films with $L2_1$ ordering than found in films with B2 ordering.[28] Our samples fabricated with the 2-step process are smoother [Fig. 4(b)] than those produced with the 1-step process. Since the contact diameter of the probe in our AR spectra experiments is only a few nm, the surface roughness, which is believed to strongly influence the MTJ characteristics, may not significantly affect our measurement results.

Our direct ARS measurements show that the *P* value of CFAS films can be as high as 80% and depends crucially on the fabrication process. This value is consistent with the large CPP GMR and TMR values reported in the literature.[6, 14–16] Our observation of a range of polarization values that can be found for films with similar magnetic properties is interesting and should provide valuable information to researchers developing spintronic devices.

In summary, we have fabricated CFAS thin-films using both the 1-step and 2-step methods and measured the sample's intrinsic spin polarization values. We find that the magnetic properties of the samples are similar, although the spin polarization is different. Spin polarization as high as 80% has been observed by Andreev reflection spectroscopy for the CFAS samples grown at room temperature followed by post annealing.

[1] S. Yuasa, T. Nagahama, A. Fukushima, Y. Suzuki, and K. Ando, Nat. Mater. **3**, 868 (2004).

[2] S. S. P. Parkin, C. Kaiser, A. Panchula, P. M. Rice, B. Hughes, M. Samant, and S. H. Yang, Nat. Mater. **3**, 862 (2004).

[3] S. Ikeda, J. Hayakawa, Y. Ashizawa, Y. M. Lee, K. Miura, H. Hasegawa, M. Tsunoda, F. Matsukura, and H. Ohno, Appl. Phys. Lett. **93**, 082508 (2008).

[4] R. A. de Groot, F. M. Mueller, P. G. van Engen, and K. H. J. Buschow, Phys. Rev. Lett. **50**, 2024 (1983).

[5] W. E. Pickett and J. S. Moodera, Phys. Today **54**, 39 (2001).

[6] R. Shan, H. Sukegawa, W. H. Wang, M. Kodzuka, T. Furubayashi, T. Ohkubo, S. Mitani, K. Inomata, and K. Hono, Phys. Rev. Lett. **102**, 246601 (2009).

[7] J. Kübler, A. R. Williams, and C. B. Sommers, Phys. Rev. B **28**, 1745 (1983).

[8] S. Fujii, S. Sugimura, S. Ishida, and S. Asano, J. Phys.: Condens. Matter **2**, 8583 (1990).

[9] S. Ishida, S. Fujii, S. Kashiwagi, and S. Asano, J. Phys. Soc. Jpn. **64**, 2152 (1995).

[10] H. C. Kandpal, G. H. Fecher, C. Felser, and G. Schönhense, Phys. Rev. B **73**, 094422 (2006).

[11] L. Ritchie, G. Xiao, Y. Ji, T. Y. Chen, C. L. Chien, M. Zhang, J. Chen, Z. Liu, G. Wu, and X. X. Zhang, Phys. Rev. B **68**, 104430 (2003).

[12] B. S. D. Ch. S. Varaprasad, A. Rajanikanth, Y. K. Takahashi, and K. Hono, Appl. Phys. Express **3**, 023002 (2010).

[13] A. Rajanikanth, Y. K. Takahashi, and K. Hono, J. Appl. Phys. **103**, 103904 (2008).

[14] T. Furubayashi, K. Kodama, H. Sukegawa, Y. K. Takahashi, K. Inomata, and K. Hono, Appl. Phys. Lett. **93**, 122507 (2008).

[15] H. Sukegawa, S. Kasai, T. Furubayashi, S. Mitani, and K. Inomata, Appl. Phys. Lett. **96**, 042508 (2010).

[16] W. Wang, H. Sukegawa, R. Shan, and K. Inomata, Appl. Phys. Lett. **93**, 182504 (2008).

[17] W. Wang, E. Liu, M. Kodzuka, H. Sukegawa, M. Wojcik, E. Jedryka, G. H. Wu, K. Inomata, S. Mitani, and Kazuhiro Hono, Phys. Rev. B **81**, 140402(R) (2010).

[18] W. H. Butler, X.-G. Zhang, T. C. Schulthess, and J. M. MacLaren, Phys. Rev. B **63**, 054416 (2001).

[19] G. J. Strijkers, Y. Ji, F. Y. Yang, C. L. Chien, and J. M. Byers, Phys. Rev. B **63**, 104510 (2001).

[20] The presence of metallic Al after oxidation will not significantly affect the tunneling measurements with the superconducting Pb electrodes. However, the Al thickness should be reduced to eliminate unwanted spin-flip scattering in the excess Al for spintronic devices.

[21] T. M. Nakatani, A. Rajanikanth, Z. Gercsi, Y. K. Takahashi, K. Inomata, and K. Hono, J. Appl. Phys. **102**, 033916 (2007).

[22] W. Wang, H. Sukegawa, R. Shan, T. Furubayashi, and K. Inomata, Appl. Phys. Lett. **92**, 221912 (2008).

[23] G. Wexler, Proc. Phys. Soc. **89**, 927 (1966).

[24] G. E. Blonder, M. Tinkham, and T. M. Klapwijk, Phys. Rev. B **25**, 4515 (1982).

[25] G. T. Woods, R. J. Soulen, Jr., I. I. Mazin, B. Nadgorny, M. S. Osofsky, J. Sanders, H. Srikanth, W. F. Egelhoff, and R. Datla, Phys. Rev. B **70**, 054416 (2004).

[26] P. Chalsani, S. K. Upadhyay, O. Ozatay, and R. A. Buhrman, Phys. Rev. B **75**, 094417 (2007).

[27] T. Y. Chen, S. X. Huang, and C. L. Chien, Phys. Rev. B **81**, 214444 (2010).

[28] T. Y. Chen, Z. Tesanovic, and C. L. Chien, Phys. Rev. Lett. **109**, 146602 (2012).

[29] N. Tezuka, N. Ikeda, A. Miyazaki, S. Sugimoto, M. Kikuchi, and K. Inomata, Appl. Phys. Lett. **89**, 112514 (2006).